

OGLE-LMC-ECL-09937: The Most Massive Algol-Type Binary System With A Mass Measurement Accurate to 2%D. M. Skowron¹, M. Kourniotis^{2,3}, J. L. Prieto^{4,5}, N. Castro⁶,
A. Z. Bonanos³, D. K. Pięnkowski¹¹ Warsaw University Observatory, Al. Ujazdowskie 4, 00-478 Warszawa, Poland
e-mail: dszczyg@astrouw.edu.pl² Astronomický ústav AVČR, Ondřejov, 25165, Czech Republic³ IAASARS, National Observatory of Athens, Penteli 15236, Greece⁴ Núcleo de Astronomía de la Facultad de Ingeniería, Universidad Diego Portales,
Av. Ejército 441, Santiago, Chile⁵ Millennium Institute of Astrophysics, Santiago, Chile⁶ Department of Astronomy, University of Michigan, 1805 S. University, Ann Arbor,
MI 48109, USA*Received December 11, 2017*

ABSTRACT

This paper presents a detailed analysis of the light and radial velocity curves of the semi-detached eclipsing binary system OGLE-LMC-ECL-09937. The system is composed of a hot, massive and luminous primary star of a late-O spectral type, and a more evolved, but less massive and luminous secondary, implying an Algol-type system that underwent a mass transfer episode. We derive masses of $21.04 \pm 0.34 M_{\odot}$ and $7.61 \pm 0.09 M_{\odot}$ and radii of $9.93 \pm 0.06 R_{\odot}$ and $9.18 \pm 0.04 R_{\odot}$, for the primary and the secondary component, respectively, which make it the most massive known Algol-type system with masses and radii of the components measured with $< 2\%$ accuracy. Consequently, the parameters of OGLE-LMC-ECL-09937 provide an important contribution to the sparsely populated high-mass end of the stellar mass distribution, and an interesting object for stellar evolution studies, being a possible progenitor of a binary system composed of two neutron stars.

Key words: *binaries: eclipsing – Stars: early-type – Stars: fundamental parameters – Stars: massive*

1. Introduction

Mass is the most important property of a star. The initial mass and metallicity to a large extent determine the whole life and fate of a star. Moreover, the evolution of the star in a binary system is significantly influenced by its companion (Sana *et al.* 2012). Most stars with well-determined masses are Galactic stars with roughly solar metallicity. Obtaining accurate parameters for stars in environments

with different metallicities is crucial for testing stellar evolutionary theories and for measuring distances to nearby galaxies (*e.g.*, Bonanos *et al.* 2006). Moreover, investigating stars in the lowest metallicity environments is a step toward exploring the early Universe and puts us closer to the Population III regime of metal-free stars (even if we lack true zero metallicity stars). The stellar mass distribution, particularly the initial mass function (IMF), is fundamental for constructing accurate models of galaxies and tracing their evolution.

The high-mass end of the stellar mass distribution is very poorly constrained, which is a serious problem for verifying theoretical models of stellar evolution. At the same time, the evolution of massive stars is violent and their deaths lead to many interesting phenomena. For example, massive binary stars are thought to be the progenitors of Gamma Ray Bursts, especially in the case of Population III stars (*e.g.*, Toma *et al.* 2016). Furthermore, procuring accurate fundamental measurements of the masses of high-mass stars is essential for determining the slope of the IMF.

The review by Torres *et al.* (2010) lists all detached binary systems of any mass in which the mass and radius of both components are measured with $\leq 3\%$ accuracy. This is the precision necessary to test models of stellar evolution, and provide constraints strong enough that models with incorrect underlying physics can be rejected. The list contains 190 individual stars, of which only two are extragalactic. The most massive star on the list is a component of V3903 Sgr which has a mass of only $27.27 M_{\odot}$, and there are only three stars with masses greater than $20 M_{\odot}$ and 17 with masses above $10 M_{\odot}$. DEBCat (Southworth 2015) is a living catalog that provides physical properties of stars in detached eclipsing binary systems that have been determined with $\leq 2\%$ accuracy. As of today, the list contains 390 stars (195 systems) and the record still belongs to V3903 Sgr. The number of stars with masses greater than $20 M_{\odot}$ is four, while with masses greater than $10 M_{\odot}$ is 22. For stars with $M > 30 M_{\odot}$ the situation is even worse, there are very few measurements accurate to less than 10% (*e.g.*, Bonanos 2009).

Motivated by the deficiency of massive stars with accurate mass measurements in low metallicity environments, we undertook a spectroscopic survey of the most luminous stars in the Large Magellanic Cloud (LMC), with an aim to measure their masses with at least 2% accuracy, necessary for precise astrophysical studies. The targets are the eight most luminous binary systems in the LMC identified by Szczygieł *et al.* (2010). In this paper, we present the analysis of the first candidate massive binary system from our sample, namely BI 98 = OGLE-LMC-ECL-09937.

This paper is organized as follows. Section 2 gives an overview of the observational data and its preparation. In Section 3 we present the process of estimating physical parameters of the system, and discuss the results in Section 4. We summarize the paper in Section 5.

2. Observations and Data Preparation

OGLE-LMC-ECL-09937 was identified by Szczygieł *et al.* (2010) in the All Sky Automated Survey (ASAS, Pojmański 1997) data as an eclipsing binary star ASAS 051230-6727.3. It is located in the LMC at $\alpha = 78^\circ.1266632$ and $\delta = -67^\circ.4539948$, has a period of 3.765184 d, magnitude $V = 14.03$ mag and amplitude of 0.62 mag. It has been assigned a B1:V spectral type by Massey *et al.* (1995) and was included in the infrared study of massive stars by Bonanos *et al.* (2009).

2.1. Photometric data

The original ASAS (Pojmański 2002) light curve of ASAS051230-6727.3 that led to its identification as an eclipsing binary (Szczygieł *et al.* 2010), is of very low quality. However, the catalog of eclipsing binaries from the OGLE survey (Graczyk *et al.* 2011) contains the high quality I - and V -band light curves of the object, extracted from the third phase of the OGLE project (Udalski *et al.* 2008). There are 476 and 40 points in the I - and V -band light curves of OGLE-LMC-ECL-09937, respectively. The data were reduced and calibrated with the standard OGLE image subtraction pipeline (Udalski 2003). Thanks to the high quality of the OGLE data we were able to refine the orbital period using the TATRY code based on the multi-harmonic periodogram of Schwarzenberg-Czerny (1996) and the new value is $P = 3.765229$ d. The corrected value of the time of primary eclipse is $HJD_0 = 2453637.487389$ d.

2.2. Spectroscopic data

Spectroscopic observations were carried out with the Du Pont 2.5 m and the Magellan Clay 6.5 m telescopes at the Las Campanas Observatory in Chile. In the Du Pont we used the Echelle spectrograph with a $1'' \times 4''$ slit and 2×2 binning, yielding a resolution of $R = 30000$, which corresponds to 10 km/s, sufficient for velocity separations of ≈ 100 km/s. Separate exposures were collected, in order to facilitate the removal of cosmic rays and artifacts. For the wavelength calibration, ThAr lamp spectra of 20 s were taken before and after each science exposure. Milky Flats and Bias frames were collected in the afternoon preceding each night. Typical signal to noise is about 60 for the combined spectra. In the Magellan Clay we used the Magellan Inamori Kyocera Echelle (MIKE; Bernstein *et al.* 2003) spectrograph with a $1''$ slit and 1×1 binning, yielding a resolution of $R = 30000$. For calibration we obtained bias frames, quartz and milky flats, and ThAr lamps for each science exposure. Table 1 provides the log of spectroscopic observations.

The Du Pont Echelle data were reduced using standard IRAF (Tody 1986, Tody 1993) packages. First, a master Bias frame was constructed from single Bias frames and subtracted from each science observation. Then a normalized Milky Flat was created from a median of single images, and corrected for bad pixels. Finally,

Table 1
Spectroscopic observations of LMC3.

| DATE | HJD | PHASE | EXPTIME | AIRMASS | S/N | TELESCOPE |
|------------|----------------|-------|------------|---------|-----|-----------------|
| 2009-12-24 | 2455189.664040 | 0.24 | 1200 s | 1.28 | 73 | Clay/MIKE |
| 2010-10-08 | 2455477.770863 | 0.75 | 3 × 1800 s | 1.41 | 35 | Du Pont/Echelle |
| 2010-10-10 | 2455479.823712 | 0.30 | 3 × 1800 s | 1.31 | 35 | Du Pont/Echelle |
| 2010-11-09 | 2455509.705694 | 0.24 | 3 × 1800 s | 1.36 | 45 | Du Pont/Echelle |
| 2011-09-02 | 2455806.872237 | 0.16 | 700 s | 1.38 | 58 | Clay/MIKE |
| 2014-01-08 | 2456665.570596 | 0.22 | 2400 s | 1.31 | 61 | Clay/MIKE |
| 2017-01-10 | 2457763.565667 | 0.83 | 3 × 1800 s | 1.31 | 55 | Du Pont/Echelle |
| 2017-01-11 | 2457764.687263 | 0.13 | 3 × 1800 s | 1.34 | 50 | Du Pont/Echelle |
| 2017-01-12 | 2457765.592431 | 0.37 | 3 × 1800 s | 1.28 | 38 | Du Pont/Echelle |

HJD is calculated for the mid-exposure of the total of all three frames

science spectra were divided by the master Milky Flat. An initial cosmic ray rejection on single images was performed using the DCR program (Pych 2004), which works well with spectroscopic data. The Clay MIKE data were reduced using the Carnegie pipeline¹, which uses similar reduction steps as described for the Du Pont Echelle reduction.

The FITS images were further processed with the `noao.imred.echelle` package from IRAF. Both science and ThAr spectra were extracted with the task `apall`. The line identification in ThAr spectra was done with the `ecidentify` and `ecreidentify` tasks and the wavelength calibration of science spectra was achieved with `refspec` and `discpcor` tasks. The spectra were normalized with the `continuum` task and merged with `scombine`. Finally, a barycentric correction was applied with the use of `rvsao.bcvcrr`.

3. Binary Modeling

3.1. Spectroscopy and radial velocities

The spectrum of OGLE-LMC-ECL-09937 is characterized by the presence of neutral helium and hydrogen lines in absorption. Both components are distinguishable, and most significant spectral lines are pictured in Figs. 1 and 2 at different orbital phases. We classify the stronger, primary component following the criteria and the optical atlas for OB stars by Walborn and Fitzpatrick (1990). The weak, questionable HeII 4200 Å implies that the star is of late-O/early-B spectral type.

¹<http://code.obs.carnegiescience.edu/mike>

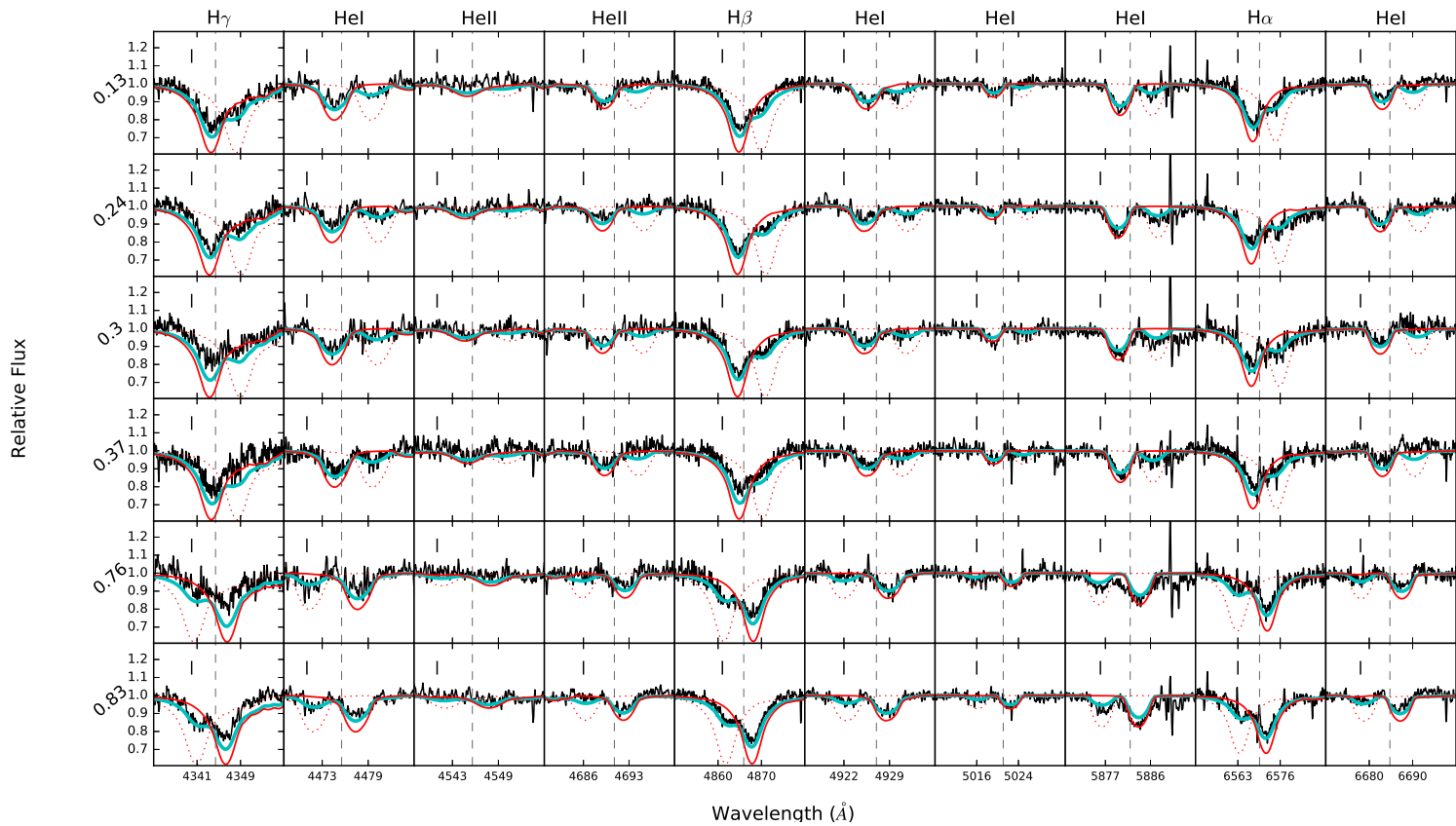


Fig. 1. Selected H and He features in Du Pont spectra of OGLE-LMC-ECL-09937 shown at different orbital phases, marked on the left. The red solid and dotted lines correspond to the primary and secondary component, respectively, shifted at their measured velocities given in Table 2. The combined fit to the observations (black line) is shown with a cyan solid line. The vertical solid line marks the rest wavelength of the spectral line, while the vertical dashed line, the location of the systemic velocity.

The low ratio HeII 4541/HeI 4471 indicates a spectral type later than O7, whereas the presence of HeII 4686 in absorption is typical for high-gravity stars earlier than B0.5. Based on these diagnostics, the primary component can be assigned a late-O main-sequence spectral type. Absorption of HeII lines is not evident for the companion thus favoring a B-type classification, although its small contribution to the total flux prevents identification of intrinsically weak lines.

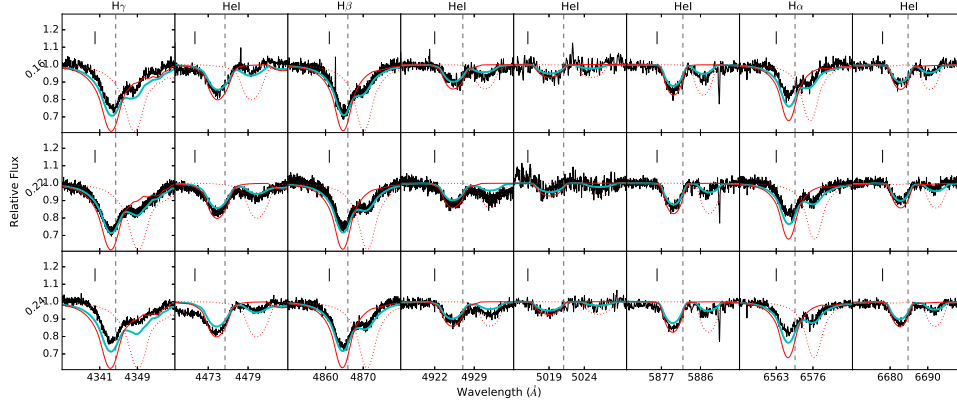


Fig. 2. Same as Fig. 1, but for the MIKE spectra. The four first features are from the BLUE arm and the four last from the RED arm of MIKE.

We proceeded to measure radial velocities (RVs) and estimate spectroscopic temperatures in two steps. First, we pursued a preliminary fit to the kinematics of the system and inferred stellar properties that would physically constrain the final selection of spectroscopic models. In a second step, we derived spectroscopic temperatures and fine-tuned the RVs throughout the phases.

We employed a set of plane-parallel, NLTE, TLUSTY high-gravity models (Hubeny and Lanz 1995) at $Z = 0.5 Z_{\odot}$, with $T_{\text{eff}} = 30000$ K consistent with the late-O/early-B spectral type of the system. To fit the observed spectra, we run a least-square minimization algorithm under a Levenberg-Marquardt scheme, setting free the RVs of the components and the flux ratio. The algorithm was run over spectral features visible for both components, namely H lines (4340 Å, 4861 Å, 6563 Å) and HeI lines (4471 Å, 4922 Å, 5016 Å, 5876 Å, 6678 Å), which were selected due to their strength and S/N ratio. The resulting RV curves along with the OGLE light curves were then processed with PHOEBE v1.0 (Prša and Zwitter 2005), which wraps the renowned Wilson-Devinney code for modeling the physics of eclipsing binaries (Wilson and Devinney 1971).

The system was initially modeled in the “detached” mode. The fit solution however, converged to the semi-detached configuration with the secondary component filling the Roche lobe, hence we switched to that configuration. A by-eye reasonable fit of the light curves was achieved from the manual adjustment of the surface potential of the primary component Ω_1 , effective temperature of the sec-

ondary T_{eff_2} , and inclination i . The mass ratio q , semi-major axis a , and systemic velocity γ were adjusted to optimally fit the RV curves. Bolometric and passband coefficients for the logarithmic limb-darkening law were taken from Van Hamme (1993). After choosing the initial values, all six parameters were set free, to allow for the built-in fit optimization of PHOEBE based on the method of differential corrections. The period and HJD_0 were fixed to the values determined from the light curve analysis.

The best-fit PHOEBE model yielded surface gravity values of 3.75 and 3.40 for the hot and cool component, respectively. The resulting V -band light ratio of 2.3 was used to fix the spectroscopic flux ratio. Having stellar models constrained by these values, we repeated the RV velocity optimization using the Du Pont observations of 2017-01-10 with the highest S/N, now setting the temperature of the models free over a grid of TLUSTY models with $T_{\text{eff}} = 19000\text{--}40000$ K. Additionally, the models were broadened over a wide range of rotational velocity values from 50 km/s to 200 km/s, with a step of 20 km/s.

We found that minimization of the residuals of the selected spectral features was achieved with a primary component temperature $T_{\text{eff}_1} = 32500$ K. The temperature of the secondary was found to be similar, but poorly constrained. Broadening of the primary was optimized at $v \sin i = 150$ km/s. Because of the 2500 K step of the TLUSTY model grid, we repeated the same process using models generated with FASTWIND stellar atmosphere code (Santolaya-Rey *et al.* 1997, Puls *et al.* 2005), which enables non-LTE calculations assuming a spherical symmetry geometry. We generated a grid of FASTWIND templates with a step of 1000 K at the inferred broadening with TLUSTY and using the gravity values from the preliminary study with PHOEBE. The best fit was achieved again with a primary temperature of 32000 ± 1600 K and a secondary of temperature 34000 ± 4000 K. Interestingly, by running the fit process for every spectrum, we derived a consistent T_{eff_1} throughout the orbital phases, whereas T_{eff_2} was largely deviating within errors from 21 000 K to even 40 000 K due to its low strength in the composite spectrum. We decided to infer T_{eff_2} from the PHOEBE model and measure RVs using two templates of 32 000 K. The resulting values are listed in Table 2 with the best-fit model displayed over the observations in Figs. 1 and 2.

3.2. Fundamental parameters of OGLE-LMC-ECL-09937

Having measured the radial velocities, we used them together with the high quality OGLE-III V - and I -band light curves to calculate the final fit parameters with PHOEBE. Since the uncertainties of the parameters provided by the GUI interface of PHOEBE are underestimated, we used the scripter to estimate their realistic values. First, we generated a 1000 bootstrap samples of both the light and radial velocity curves. The light curves were created by k -multicombination of the original light curve consisting of k points (where k is 476 and 40 for the I - and V -band, respectively). Due to the small number of points, the RV curves were created

Table 2

Radial velocity measurements for OGLE-LMC-ECL-09937

| HJD | RV ₁ (km/s) | RV ₂ (km/s) | PHASE | TELESCOPE |
|----------------|------------------------|------------------------|-------|-----------------|
| 2455189.664040 | 194 (4) | 599 (8) | 0.24 | Clay/MIKE BLUE |
| | 198 (4) | 618 (8) | | Clay/MIKE RED |
| 2455477.770863 | 419 (4) | -2 (10) | 0.76 | Du Pont/Echelle |
| 2455479.823712 | 196 (4) | 589 (10) | 0.30 | Du Pont/Echelle |
| 2455509.705694 | 195 (4) | 599 (8) | 0.24 | Du Pont/Echelle |
| 2455806.872237 | 206 (4) | 546 (8) | 0.16 | Clay/MIKE BLUE |
| | 207 (6) | 557 (12) | | Clay/MIKE RED |
| 2456665.570596 | 200 (4) | 603 (4) | 0.22 | Clay/MIKE BLUE |
| | 207 (4) | 628 (6) | | Clay/MIKE RED |
| 2457763.565667 | 403 (4) | 29 (8) | 0.83 | Du Pont/Echelle |
| 2457764.687263 | 215 (4) | 537 (8) | 0.13 | Du Pont/Echelle |
| 2457765.592431 | 218 (4) | 550 (6) | 0.37 | Du Pont/Echelle |

Uncertainties (2σ) are given in parentheses.

by randomly selecting each point within its 2σ uncertainty around the measured value (listed in Table 2), assuming a Gaussian distribution. The temperature of the primary was also randomized over its spectroscopic value 32000 ± 1600 K. We then ran PHOEBE on each of the 1000 bootstrap samples and derived 1000 sets of parameters of the system. The mean values of the parameters and their 1σ uncertainties are listed in Table 3 and the resulting PHOEBE model is shown in Fig. 3. The fundamental parameters of the components are given in Table 4. We derived masses of $21.03 \pm 0.34 M_{\odot}$ and $7.64 \pm 0.09 M_{\odot}$ and radii of $9.65 \pm 0.08 R_{\odot}$ and $9.20 \pm 0.03 R_{\odot}$, for the primary and the secondary component, respectively. The surface temperature of the secondary is measured to be $T_{\text{eff}_2} = 21800 \pm 1200$ K, which is marginally consistent with the poorly determined spectroscopic one.

3.3. Spot model

The resulting best-fit light curve model from PHOEBE shows room for further improvement (see Fig. 3 and the left panel of Fig. 4). The suppression of the photometric baseline in both the *I*- and *V*-band light curves prior to the occultation of the primary implies the presence of an additional cool component. Since spots are expected in stars of later types than the one studied here, we attribute the observed fluctuation in the light curve to the reflection effect, in which the hotter primary heats the facing surface of the secondary, increasing its effective temperature. The temperature of the unreflected region on the secondary (*i.e.*, the projected surface of the secondary at phase zero) would then indicate the actual T_{eff_2} value.

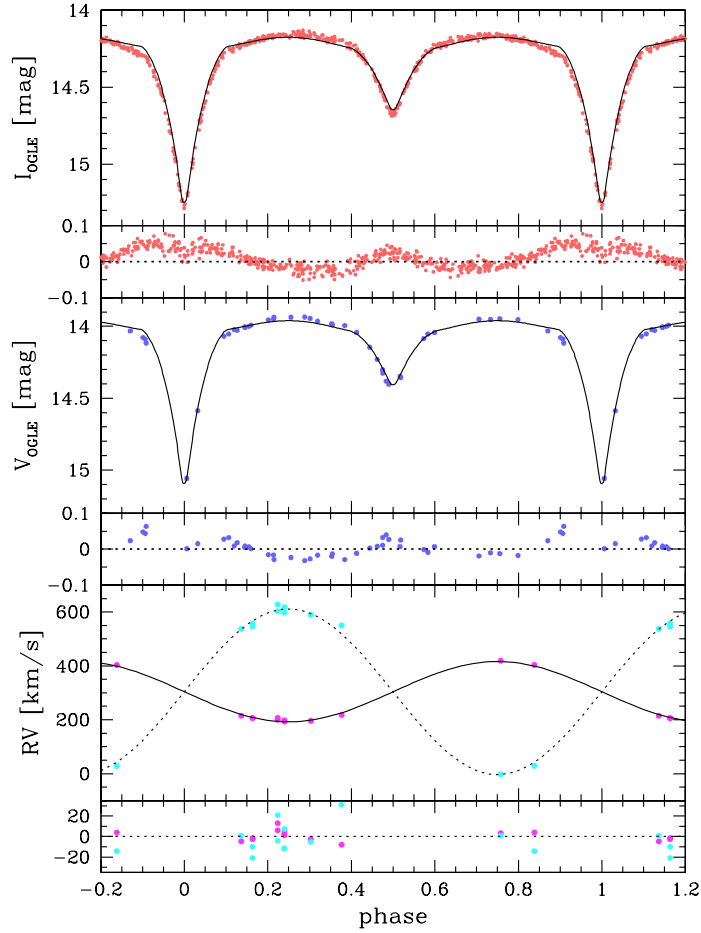


Fig. 3. Light curves and radial velocity curves of the best fit model with PHOEBE. The *top* and *middle panels* show the *I*- and *V*-band OGLE-III light curves, respectively, together with residuals. The *bottom panel* shows the RV curve of the primary (magenta) and the secondary (cyan) with the best fit model for the primary (solid line) and secondary (dotted line), and the residuals.

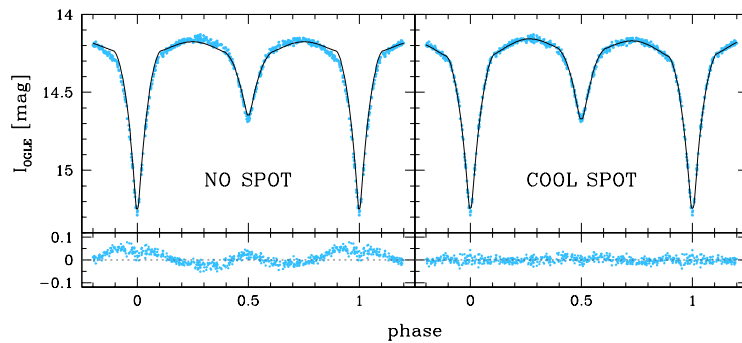


Fig. 4. Comparison of two light curve models from PHOEBE – without a cool spot (*left panel*) and with the spot (*right panel*). Blue dots in the top panels show the OGLE-III *I*-band light curve, while the black line denotes the model. *Bottom panels* show the residuals between the data and the model.

Table 3

Parameters of the OGLE-LMC-ECL-09937 system measured with PHOEBE

| Parameter | Unit | Non-Spot Model | Spot Model ^(a) |
|--|-----------------|----------------------------|---------------------------|
| Period P | [d] | 3.765229 ± 0.000003 | |
| HJD ₀ | [d] | 2453637.48739 ± 0.0002 | |
| Semimajor axis, a | [R_{\odot}] | 31.2 ± 0.1 | 31.2 ± 0.1 |
| Systemic velocity, γ | [km/s] | 304 ± 1 | 304 ± 1 |
| Inclination, i | [deg] | 90.0 ± 0.4 | 89.6 ± 0.4 |
| Mass ratio, q | | 0.364 ± 0.004 | 0.362 ± 0.004 |
| Surface potential of the primary, Ω_1 | | 3.64 ± 0.02 | 3.55 ± 0.02 |
| Flux ratio in the V -band | | 2.25 ± 0.05 | 1.90 ± 0.02 |
| Flux ratio in the I -band | | 2.08 ± 0.04 | 1.80 ± 0.02 |

(a) A spot with longitude 190° , a radius of 70° , and a temperature 0.86 of the stellar surface.

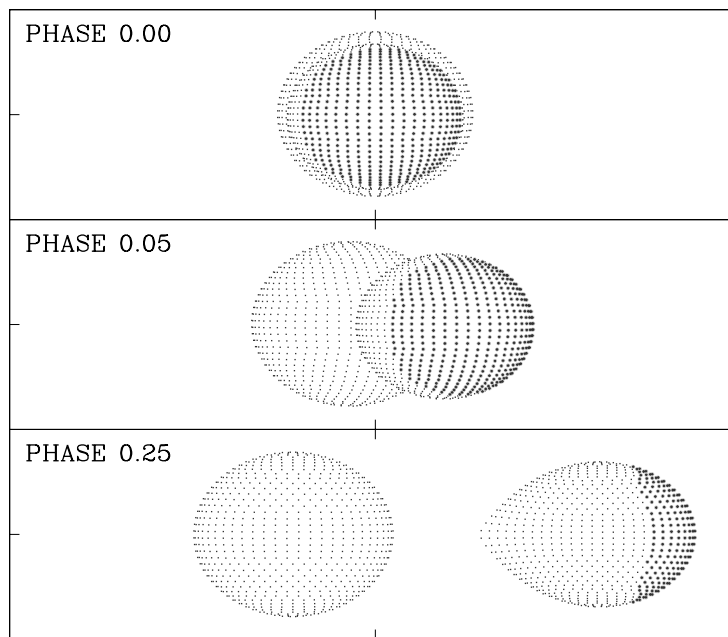


Fig. 5. Location of the large cool spot on the secondary star is shown on a mesh plot imported from PHOEBE at three different orbital phases.

Once again we used PHOEBE to model the system, this time with the addition of a large “cool spot” on the secondary star, that would imitate the reflection effect. We assumed an equatorial location of the spot, *i.e.*, the colatitude of 90° . The remaining three parameters of the spot: longitude, radius, and temperature were determined via multiple fit iterations; each time a different set of the spot parameters from a wide range of values was chosen, the observations were fit, and the

χ^2 value was returned. The longitude of the spot of 190° as measured from the L1 point was found to yield the lowest χ^2 values. The fact that these two points are not anti-diametrical, is believed to be due to rotation. For spot radii above 60° , the optimization of the fit models was achieved for a spot temperature of 0.86 of that of the stellar surface. Assuming a spot radius of 70° , spanning the entire projected surface of the secondary at phase zero (see Fig. 5), we fixed the three parameters to the above values and repeated the iterative fit process described in Section 3.2.

The updated parameters of the model are also listed in Table 3 with the new model shown in the right panel of Fig. 4. The residuals of the fit are greatly improved when compared to the non-spot model, indicating a good model selection. The fundamental parameters of the updated model with the spot are given in the right column of Table 4. The updated masses are $21.04 \pm 0.34 M_\odot$ and $7.61 \pm 0.09 M_\odot$ for the primary and the secondary component, respectively, which are well consistent, within their 1–2% precision, with those derived from the previously discussed non-spot model.

Table 4

Fundamental parameters of the components of OGLE-LMC-ECL-09937 measured with PHOEBE

| Parameter | Unit | Non-Spot Model | Spot Model ^(a) |
|--------------------------------|-------------|-------------------|---------------------------|
| Mass of the primary, M_1 | $[M_\odot]$ | 21.03 ± 0.34 | 21.04 ± 0.34 |
| Mass of the secondary, M_2 | $[M_\odot]$ | 7.64 ± 0.09 | 7.61 ± 0.09 |
| Radius of the primary, R_1 | $[R_\odot]$ | 9.65 ± 0.08 | 9.93 ± 0.06 |
| Radius of the secondary, R_2 | $[R_\odot]$ | 9.20 ± 0.03 | 9.18 ± 0.04 |
| $T_{\text{eff}1}$ | [K] | 32000 ± 1600 | 32000 ± 1600 |
| $T_{\text{eff}2}$ | [K] | 21800 ± 1200 | $21100 \pm 1400^{(b)}$ |
| $\log(g_1)$ | | 3.791 ± 0.008 | 3.767 ± 0.006 |
| $\log(g_2)$ | | 3.394 ± 0.002 | 3.393 ± 0.002 |
| $\log(L_1/L_\odot)$ | | 4.94 ± 0.09 | 4.96 ± 0.09 |
| $\log(L_2/L_\odot)$ | | 4.23 ± 0.10 | 4.17 ± 0.10 |

(a) A spot with longitude 190° , a radius of 70° , and a temperature 0.86 of the stellar surface.

(b) The temperature of the cool spot, *i.e.*, unreflected region.

4. Discussion

By comparing dynamical masses to the predicted evolutionary ones, eclipsing binaries with spectroscopically measured parameters serve as a unique tool for evaluating the current theoretical models. We employed stellar evolutionary models and isochrones from MESA Isochrones and Stellar Tracks (MIST) v.1.1. (Dotter 2016, Choi *et al.* 2016, Paxton *et al.* 2011), assuming rotation at the 40% of the critical velocity. The metallicity of the models was set to the average value

of $[\text{Fe}/\text{H}] = -0.39$ dex for the LMC, which is measured from the calibration of the spectroscopic data of Red Giant Branch stars (Choudhury *et al.* 2016). Stellar tracks for masses of $8 M_{\odot}$ to $24 M_{\odot}$ and isochrones of 1 Myr, 3 Myr, 5 Myr, 10 Myr, and 30 Myr, are shown on the Hertzsprung-Russell diagram of Fig. 6. The black squares show the location of the components on the diagram, as inferred from our modeling with PHOEBE with the addition of the cool, unreflected region.

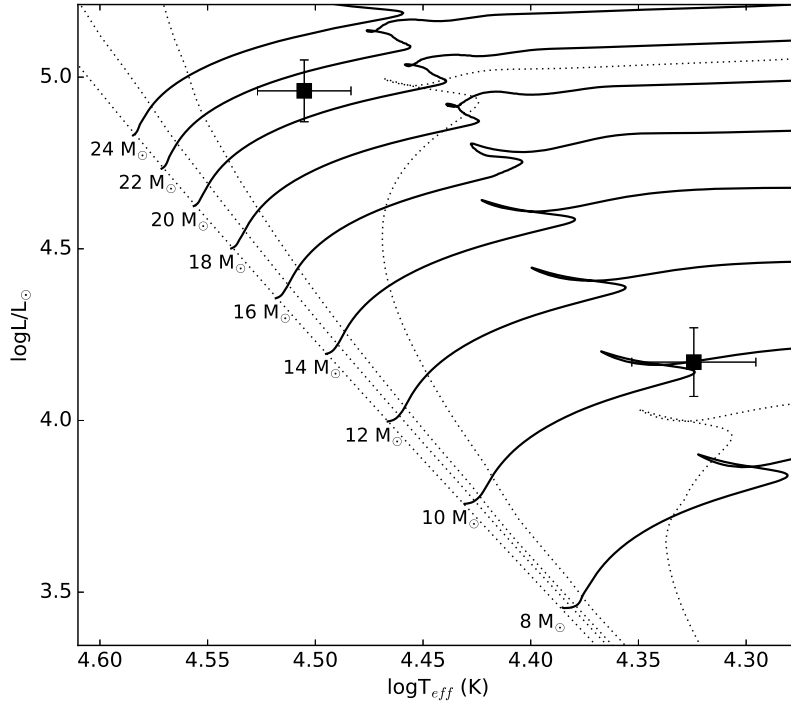


Fig. 6. Hertzsprung–Russell diagram for the components of OGLE-LMC-ECL-09937 (black squares) studied with PHOEBE. We show MESA evolutionary stellar tracks for initial masses $8 M_{\odot}$ to $24 M_{\odot}$, assuming rotation at 40% of the critical velocity. Isochrones of 1 Myr, 3 Myr, 5 Myr, 10 Myr, and 30 Myr are shown with dotted lines.

We find a good agreement between the evolutionary and dynamical mass of $21 M_{\odot}$ for the primary component, which appears to reside well within the main-sequence strip. The secondary component is found to be $\approx 30\%$ overluminous for its mass and further indicates an evolved state not far beyond the main sequence. As the cooler, fainter, and less massive secondary is found to fill the Roche lobe, it is reasonable to consider the system as an Algol-type binary (Giuricin *et al.* 1983). Accordingly, the secondary should have been initially a massive early-type star that underwent a rapid mass transfer to its companion, which is now the more massive and luminous primary (Peters 2001). The agreement between the primary mass and its theoretical single-evolved counterpart could imply that the gainer had enough time to stabilize to its present state and that the mass transfer is currently absent.

In an attempt to detect possible changes in the orbital period, that would suggest an ongoing mass transfer, we calculated the orbital period of the system separately for each OGLE observing season. In order to extend the baseline of the observations, we supplemented the OGLE-III *I*-band light curve with the OGLE-IV (Udalski *et al.* 2015) data from the catalog of eclipsing binaries by Pawlak *et al.* (2016). The combined dataset spans over 14 years of observations (14 observing seasons). Furthermore, we downloaded the *V*-band light curve of OGLE-LMC-ECL-09937 from the All-Sky Automated Survey for Supernovae (ASAS-SN, Shappee *et al.* 2014) using the ASAS-SN Light Curve Server (Kochanek *et al.* 2017), spanning over 3.5 years of observations in four observing seasons. This further extended the baseline to almost 17 years. We calculated an accurate period value for each of the observing seasons within OGLE-III and ASAS-SN data and for each two seasons in OGLE-IV data (due to fewer points) with the TATRY code and found no evident variability in the period within uncertainties.

OGLE-LMC-ECL-09937 is one of the few massive Algol-type systems with an accurate mass measurement of 2%. In Fig. 7, we show the mass–radius plot for the components of the Algol-type systems from the catalog of Budding *et al.* (2004) updated with the most recent mass values for the components of the massive system ET Tau (Williamon *et al.* 2016). Light gray dots represent stars for which there is no error estimate for the mass, dark gray dots stand for stars for which the error on the mass is more than 2%, and large black circles mark the stars for which masses were determined with up to 2% accuracy. The most massive binary in the catalog is RY Sct, which has had a number of mass measurements over the past decades, ranging from $8 M_{\odot} + 26 M_{\odot}$ (Skulskii 1992) to $36 M_{\odot} + 46 M_{\odot}$ (Cowley and Hutchings 1976). The more recent estimates oscillate around $\approx 10 M_{\odot} + 30 M_{\odot}$ but rarely provide any radii measurement. Hence we adopt the newest result by Grundstrom *et al.* (2007) of $7.1 \pm 1.2 M_{\odot}$ and $30.0 \pm 2.1 M_{\odot}$. Since the radius is not well defined, we follow Grundstrom *et al.* (2007) and adopt the radii of $18 R_{\odot}$ and $9.6 R_{\odot}$, respectively.

Fig. 7 shows that the primary component of OGLE-LMC-ECL-09937 (black square) is not only the second most massive known star in an Algol-type system, but it is also the most massive Algol component with $\leq 2\%$ accurate mass measurements. It is also one of the few massive stars with accurate physical parameters, making it an important ingredient of the stellar mass distribution and an excellent target for verifying stellar evolution scenarios of semi-detached systems.

5. Summary

This paper presents a detailed analysis of the photometric and spectroscopic data on the semi-detached eclipsing binary system OGLE-LMC-ECL-09937. The spectra of the system show lines of both components, allowing to determine both radial velocity curves, which together with the excellent quality OGLE *I*- and *V*-band

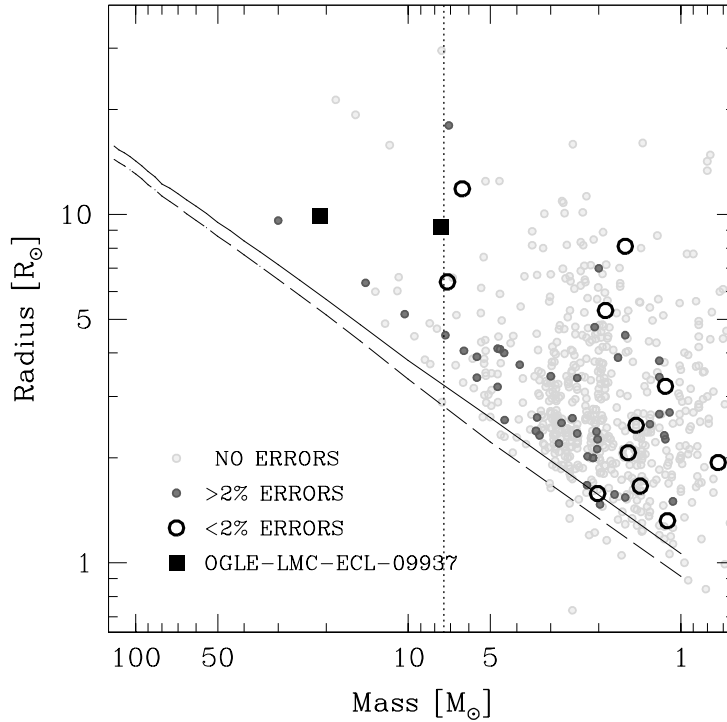


Fig. 7. Mass–radius plot for the components of known Algol-type systems. Light gray dots represent stars, for which there is no error estimate for the mass, dark gray dots represent stars, for which the error on the mass is more than 2%, and large black circles mark the stars for which masses were determined with up to 2% accuracy. The black square represents masses of the components of OGLE-LMC-ECL-09937. The solid line denotes the zero-age main sequence at the Galactic metallicity and the dashed at the LMC metallicity, taken from MIST (Dotter 2016, Choi *et al.* 2016, Paxton *et al.* 2011). The vertical dotted line drawn at $M = 7.5 M_{\odot}$ represents the limit above which there are no Algol-type component masses known with $\leq 2\%$ uncertainty.

light curves, allowed us to obtain an accurate model of the system using PHOEBE. The system is composed of a hot, massive and luminous primary star of an early B type, and a more evolved, but less massive and luminous secondary, implying an Algol-type system that underwent a mass transfer episode.

Further modeling of the binary shows that the light curve fit is greatly improved when adding a large cool region on the secondary, which is attributed to the reflection effect. The physical parameters of the system derived from the non-spotted and cool spot models are consistent within their errors. We derive masses of $21.04 \pm 0.34 M_{\odot}$ and $7.61 \pm 0.09 M_{\odot}$ and radii of $9.93 \pm 0.06 R_{\odot}$ and $9.18 \pm 0.04 R_{\odot}$, for the primary and the secondary component, respectively.

The $< 2\%$ accuracy of the mass and radius measurements make OGLE-LMC-ECL-09937 an important contribution to the sparsely populated high-mass end of the stellar mass distribution, and an interesting object for stellar evolution studies, as a potential progenitor of a binary system composed of two neutron stars.

Acknowledgements. We thank Kris Stanek for initiating and supporting this project. D.M.S and M.K. are supported by the Polish Ministry of Science and Higher Education under the grant “Iuventus Plus” No. 0420/IP3/2015/73. D.M.S. is supported by the Polish National Science Center (NCN) under the grant no. 2013/11/D/ST9/03445 and the NCN grant MAESTRO 2014/14/A/ST9/00121 to Andrzej Udalski. Support for J.L.P. is provided in part by FONDECYT through the grant 1151445 and by the Ministry of Economy, Development, and Tourism’s Millennium Science Initiative through grant IC120009, awarded to The Millennium Institute of Astrophysics, MAS.

REFERENCES

- Bernstein, R., Shectman, S. A., Gunnels, S. M., Mochmacki, S., Athey, A. E. 2003, *SPIE*, **4841**, 1694.
 Bonanos, A. Z., *et al.* 2006, *ApJ*, **652**, 313.
 Bonanos, A. Z. 2009, *ApJ*, **691**, 407.
 Bonanos, A. Z., *et al.* 2009, *AJ*, **138**, 1003.
 Budding, E., Erdem, A., Çiçek, C., Bulut, I., Soyduğan, F., Soyduğan, E., Bakiş, V., Demircan, O. 2004, *A&A*, **417**, 263.
 Choi, J., Dotter, A., Conroy, C., Cantiello, M., Paxton, B., Johnson, B. 2016, *ApJ*, **823**, 102.
 Choudhury, S., Subramaniam, A., Cole, A. 2016, *MNRAS*, **455**, 1855.
 Conti, P. 1971, *ApJ*, **170**, 325.
 Cowley, A. P., Hutchings, J. B. 1976, *PASP*, **88**, 456.
 Dotter, A. 2016, *ApJ*, **222**, 8.
 Giuricin, G., Mardirossian, F., Mezzetti, M. 1983, *ApJS*, **52**, 35.
 Graczyk, D., *et al.* 2011, *Acta Astron.*, **61**, 103.
 Grundstrom, E. D., Gies, D. R., Hillwig, T. C., McSwain, M. V., Smith, N., Gehrz, R. D., Stahl, O., Kaufer, A. 2007, *ApJ*, **667**, 505.
 Hubeny, I., Lanz, T. 1995, *ApJ*, **439**, 875.
 Kochanek, C. S. *et al.* 2017, *PASP*, **129**, 4502.
 Massey, P., Lang, C. C., Degioia-Eastwood, K., Garmany, C. D. 1995, *ApJ*, **438**, 188.
 Pawlak, M., *et al.* 2016, *Acta Astron.*, **66**, 421.
 Paxton, B., Bildsten, L., Dotter, A., Herwig, F., Lesaffre, P., Timmes, F. 2011, *ApJ*, **192**, 3.
 Peters, G. J. 2001, *ASSL*, **264**, 79.
 Pojmański, G. 1997, *Acta Astron.*, **47**, 467.
 Pojmański, G. 2002, *Acta Astron.*, **52**, 397.
 Prša, A., and Zwitter, T. 2005, *ApJ*, **628**, 426.
 Puls, J., Urbaneja, M. A., Venero, R., Repolust, T., Springmann, U., Jokuthy, A., Mokiem, M. R. 2005, *A&A*, **435**, 669.
 Pych, W. 2004, *PASP*, **116**, 148.
 Sana, H. *et al.* 2012, *Sci*, **337**, 444.
 Santolaya-Rey, A. E., Puls, J., Herrero, A. 1997, *A&A*, **323**, 488.
 Schwarzenberg-Czerny, A. 1996, *ApJ*, **460**, L107.
 Shappee, B. J. *et al.* 2014, *ApJ*, **788**, 48.
 Skulskii, M. Y. 1992, *SvA*, **36**, 411.
 Southworth, J. 2015, *ASPC*, **496**, 164.
 Szczygieł, D. M., Stanek, K. Z., Bonanos, A. Z., Pojmański, G., Pilecki, B., Prieto, J. L. 2010, *AJ*, **140**, 14.
 Tody, D. 1986, *SPIE*, **627**, 733.
 Tody, D. 1993, *ASPC*, **52**, 173.
 Toma, K., Yoon, S-C., Bromm, V. 2016, *SSRv*, **202**, 159.

- Torres, G., Andersen, J., Giménez, A. 2010, *AARv*, **18**, 67.
Udalski, A. 2003, *Acta Astron.*, **53**, 291.
Udalski, A., Szymański, M. K., Soszyński, I., Poleski, R. 2008, *Acta Astron.*, **58**, 69.
Udalski, A., Szymański, M. K., and Szymański, G. 2015, *Acta Astron.*, **65**, 1.
van Hamme, W. 1993, *AJ*, **106**, 2096.
Walborn, N. R., Fitzpatrick, E. L. 1990, *PASP*, **102**, 379.
Williamon, R. *et al.* 2016, *PASP*, **128**, 4202.
Wilson, R. E., Devinney, E. J. 1971, *ApJ*, **166**, 605.
van Hamme, W. 1993, *AJ*, **106**, 2096.